2015

Analytical Modeling of the Interface between Lightly Roughened Hollowcore Slabs and Cast-In-Place Concrete Topping

Aiham Adawi
Western University

Maged A. Youssef
Western University, youssef@uwo.ca

Mohamed E. Meshaly
Alexandria University

ANALYTICAL MODELING OF THE INTERFACE BETWEEN LIGHTLY-ROUGHENED HOLLOWCORE SLABS AND CAST-IN-SITU CONCRETE TOPPING

Aiham Adawi[1], Maged A. Youssef[2], Mohamed Meshaly [3]

[1]Ph.D. Candidate, [2]Associate Professor, [3]Visiting Researcher
Department of Civil and Environmental Engineering, Western University, London, Ontario, Canada, N6A 5B9

ABSTRACT

Hollowcore slabs are commonly used in different types of structures. They are usually topped with a 50 mm concrete topping. Structural engineers can use this topping to increase the slab load carrying capacity. North American design standards relate the horizontal shear strength at the interface between hollowcore slabs and the concrete topping to the slab surface roughness. This paper presents results of four push-off tests on hollowcore slabs supplied by two manufacturers and roughened using a conventional steel broom. The tested slabs sustained higher horizontal shear stresses than those specified by the design standards. Utilizing the data from the push-off tests, an analytical model was applied to evaluate the shear and peel stiffnesses, k_s and k_p, of the interface between hollowcore slabs and concrete topping. Structural engineers can utilize k_s and k_p values to model the composite action between hollowcore slabs from the two manufacturers and concrete topping. The analytical model was also used to evaluate the actual distribution of shear and peel stresses.

Subject Headings: shear stress, peel stress, hollowcore slabs, concrete topping, push-off tests, analytical modeling.

INTRODUCTION

Hollowcore slabs are precast/prestressed concrete elements that are commonly used in the construction industry. They are manufactured at a precast concrete plant prior to shipping to the job site. After installation, they are typically topped with a 50 mm cast-in-place concrete topping to level the surface. Structural engineers can make use of the concrete topping to increase the load carrying capacity of the slab. This consideration requires that failure at the interface between the hollowcore slab and the concrete topping does not initiate prior to reaching the ultimate capacity of the composite section. North American design standards specify that the shear strength of the interface between intentionally roughened hollowcore slab surface and the concrete topping can be taken as 0.70 MPa, CSA A23.3-04[1] clause 17.4.3.2, or 0.55 MPa, ACI 318-08[2] clause 17.5.3.1. ACI 318-08 commentary clause R17.5.3.3 defines "intentionally roughened" as a 6.4 mm of surface roughness and CSA A23.3-04 explanatory note N17.4.3.2[1] defines it as roughness to amplitude of 5.0 mm. In North America, hollowcore slabs are commonly produced using the extrusion process, which involves the use of zero-slump concrete mix and high vibration augers. The surface of hollowcore slabs manufactured using this process is referred to as "machine-cast-finish". The roughness of this surface varies depending on number of factors including: concrete mix design and wear and tear of the concrete extrusion machine. The same variability exists when this surface is roughened. Roughening a hollowcore slab surface to the amplitudes specified in the design standards involves additional time, material and labor that manufacturers would be keen to avoid. A simple roughening technique that is widely used by manufacturers involves the use of a steel broom. However, the produced roughness does not qualify the slabs to be ranked as "intentionally roughened".

The shear strength provided at the interface between hollowcore slabs and the concrete topping was investigated using full-scale tests for different surface finishes[3, 4]. The test results provided evidence that horizontal shear levels given in ACI 318[2] are highly conservative. Girhammar and Pajari (2008)[5] reported that the composite action increases the shear capacity of hollowcore slabs by 35%. Ibrahim and Elliot (2006)[6] studied the horizontal shear along the interface between hollowcore slabs and concrete topping for smooth and roughened specimens. Roughness was achieved using a steel wire brush. Moisture condition of the slab specimens before casting of the concrete topping was also a factor in the study. The study evaluated the shear capacity of the composite slabs using push-off tests. It was concluded that the roughness of the slabs was not significant to differentiate between "smooth" and "roughened" surfaces. However, surface moisture condition considerably affected the results, where dry and ponded surfaces achieved lower values compared with the wet surfaces.

This paper investigates the shear and peel behavior at the interface between hollowcore slabs and cast-in-situ concrete topping through four push-off tests. The tested hollowcore slabs have roughened surface finish. The paper then models the shear and peel stresses along the interface between the hollowcore slab specimen and the concrete topping. The model is based on the technique presented by El Damatty and Abushagur[7] to calculate the shear and peel stresses in the adhesive attaching FRP sheets to the flanges of steel I beams. A closed form solution of the system equilibrium was used to determine the distribution of the developed shear and peel stresses.

.

EXPERIMENTAL PROGRAM

Four 1219 mm by 1219 mm by 203 mm thick hollowcore slabs obtained from two manufacturers (A, B) were tested. Their surfaces were roughened using a conventional steel broom as shown in Fig. 1a. The depth of the produced random grooves was about 1 mm and each manufacturer had its own pattern as shown in Figs. 1b and 1c.

The manufacturer specified concrete compressive strength was 41 MPa. Fig. 2 shows 50 mm cubes that were sampled from the edges of each slab. Testing these cubes according to ASTM C349[9] and calculating the equivalent average cylinder concrete compressive strength showed that the actual strength was 53 MPa and 58 MPa for slabs from manufacturer A and B, respectively. Each of the tested slabs had four-½" prestressing strands.

The concrete topping properties were chosen to simulate general practice for this type of construction. Its thickness was 50 mm and it covered an area of 508 mm by 508 mm. The surfaces of the hollowcore slabs were wetted and then left to dry to obtain a "saturated dry surface" condition before casting of the topping. This prevented the water of the concrete topping to infiltrate into the hollowcore slab surface and produce a weak interface surface. The concrete mix was provided by a ready mix manufacturer and contained 10 mm pea stone aggregates and normal Portland cement. Neither air entraining agents nor additives were used. The measured average slump was 120 mm. The concrete topping did not contain any reinforcing bars to match the industry practice. Formwork and casting of the concrete topping are illustrated in Figs. 3a and 3b. Curing was done according to CSA A23.1-09[8] for class "N" exposure by wet curing for three days in the laboratory environment. Three concrete cylinders were tested according to ASTM C39[10] to evaluate the compressive strength of the concrete topping on the day of the push-off tests. The average strength was found to be 30 MPa.

Push-off Tests

The push-off tests were conducted in the vertical orientation. Fig. 4a shows a schematic of the test setup where the hollowcore slab was installed in the vertical direction with the concrete topping resting on 50 mm thick steel plate. The shear force was applied by the MTS hydraulic actuator on a spreader steel beam that pushed the hollowcore slab specimen downward. The steel plate reacted by a force on the concrete topping. This force generated shear and peel stresses along the interface between the hollowcore slab and the topping. The steel frame positioned in the back of the hollowcore specimen was designed to prevent the overturning of the test specimen. The soffit of the hollowcore slab specimen was sufficiently smooth to allow free movement of the steel frame without providing additional resistance. 50 mm wide by 3.2 mm thick Korolath brand bearing pads were used under the steel spreader beam and between the steel plate and the concrete topping to guarantee a uniform stress distribution at those locations. Fig. 4b shows a photo of the final test setup.

To capture the state of strains in the concrete topping, strain gauges were attached to its top surface as illustrated in Fig. 5. Three strain gauges (S1, S3, and S5) were installed along the vertical centerline to measure strains in the direction of the applied load. Strain gauges S2 and S4 were installed to evaluate the stress distribution across the width of the slab. The push-off tests induced two types of stresses on the interface between the concrete topping and the hollowcore slab: shear and peel stresses. Four Linear Variable Displacement Transducers (LVDTs) were used to measure movements in the shear (L3 and L4) and peel (L1 and L2) directions. LVDTs (L3 and L4) were attached to the hollowcore slab with their armatures resting on angle brackets attached to the side of the concrete topping. This setup allowed LVDTs to read the differential displacement between the hollowcore slab and the concrete topping.

Prior to starting the test, a careful visual inspection did not reveal any signs of separation between the concrete topping and the hollowcore slabs. The load was applied via the hydraulic actuator at a rate of 10 kN/minute. Displacement and strain readings were collected throughout the tests.

Test Results and Discussion

The ultimate load, at which the concrete topping separates from the hollowcore slab, and the corresponding average shear strength, $\nu_{h\text{ avg.}}$, are shown in Table 1. To obtain a conservative estimate of $\nu_{h\text{ avg.}}$, the effect of slippage on the contact area was not accounted for and, thus, $\nu_{h\text{ avg.}}$ was directly calculated by dividing the failure load by the contact area. The ultimate load accounts for the weight of the slab and the steel spreader beam. The average horizontal shear strength for all of the tested slabs was higher than the limit of 0.7 MPa and 0.55 MPa required by CSA A23.3[1] and ACI 318[2], respectively. Slabs from manufacturer A (slabs A1 and A2) demonstrated considerably higher shear strength than those from manufacturer B (slabs B1 and B2). This difference might be due to the initial surface roughness and/or the roughening pattern.

Strains recorded by S2, S3 and S4 showed close agreement in terms of values and trends as illustrated in Fig. 6 considering slab A1. Slight misalignment of the strain gauges with the load direction might have led to the shown differences. This close agreement indicates that the stresses were uniform across the slab width. Extremely brittle and abrupt failure was observed for all of the tested specimens. Load versus slip curves are shown in Fig. 7. The slip values represent the average reading of LVDTs L3 and L4. The maximum difference between the readings of LVDTs L3 and L4 was less than 10% for all slabs. The curves generally illustrate two stages; pre-yielding stage where the slope is considerably high followed by a post-yielding stage where the slope becomes flatter. While the interface capacity in the pre-yielding stage depends on the bond between the concrete topping and the hollowcore slab, the post-yielding behavior is governed by shear friction between the slab and the topping. Slabs A1 and A2 differ in the initial loading stage where slab A1 showed lower bond strength than slab A2. However, both slabs failed at similar loads. Slabs B1 and B2 had also failed at similar loads.

The abrupt failure type that was observed for all tested specimens emphasizes that the horizontal stress transferred along the interface layer did not have the ability to fully redistribute over the contact area once failure was initiated. This observation suggests that the reported values of average shear stresses are lower than the actual shear stresses that were reached.

ANALYTICAL MODEL

The hollowcore slabs are modeled as rigid elements. Two continuous spring systems were used to simulate the stiffness of the interface layer as illustrated in Fig. 8. Similar modeling technique was used by El Damatty and Abushagur7 while modeling the adhesive attaching FRP sheets to steel I beams. The first set of springs depicts the in-plane stiffness k_s in the direction of the applied load (parallel to the X axis). They allow modeling the horizontal shear stress behavior. The out-of-plane stiffness k_p models the peel behavior using another set of springs that are parallel to the Z axis. The shear stress profile $v_h(x)$ acting along the interface between the hollowcore slab and the concrete topping can be calculated using Eq. 1, where $u(x)$ is the in-plane displacement profile of the concrete topping along the X axis.

$$v_h(x) = k_s \times u(x) \quad \text{.....} \quad (1)$$

In the following sections, in-plane and out-of-plane equilibrium analysis are conducted on an infinitesimal segment of the concrete topping "element T" to evaluate the shear and peel stiffnesses k_s and k_p.

In-Plane Equilibrium

When the hollowcore slab is pushed downward by the applied force P_{hc}, an equivalent reaction force P_t is generated in the concrete topping as shown in Fig. 9. The resultant of the developed axial stresses in the concrete topping, σ, is acting at its centroid. σ has a value of zero at the top point of the topping (x = 0) and a maximum value at the bottom point (x = 508 mm).

Considering the in-plane equilibrium of an infinitesimal element T, the increase in axial stresses $d\sigma$ is in equilibrium with the developed shear stresses at the interface. The force in the in-plane spring, F_s, represents the shear force along the interface between the hollowcore slab and the concrete topping. This force can be calculated from the summation of forces along the X axis as given by Eq. 2. F_s can also be calculated as a function of the shear spring stiffness as given by Eq. 3.

$$F_s = d\sigma \times b \times t \quad \text{(2)}$$

$$F_s = K_s \times u(x) \times b \times dx \quad \text{(3)}$$

The relationship between σ and the in-plane displacement *u(x)* can be obtained from Eqs. 2 and 3 and Hook's Law as illustrated in Eqs. 4 and 5.

$$\frac{d\sigma}{dx} = k_s \times u(x) \times \frac{1}{t} \quad \text{(4)}$$

$$\sigma = E_C \times \frac{du}{dx}$$

(5)

where (du/dx) is the strain in the concrete topping, and E_c is the modulus of elasticity of concrete. Since the concrete topping is made of normal density concrete and have a compressive strength f'_c of 30 MPa, E_c is calculated using clause 8.6.2.3 of CSA A23.3-4[1]. The differential equation that governs the state of stresses in the concrete topping is:

$$\frac{d^2u}{dx^2} - \omega^2 u(x) = 0 \quad \text{(6)}$$

where $\omega^2 = \left(\frac{k_s}{tE_C}\right)$

(7)

Eq. 6 is a second order differential equation and can be solved by defining the following boundary conditions:

(1) At $x = 0 \rightarrow \frac{du}{dx} = 0$ (strain = 0)

(2) At $x = L \rightarrow \frac{du}{dx} = -\frac{P_t}{btE_c}$ (strain from Hook's Law)

Solving Eq. 6 using the defined boundary conditions leads to the following in-plane displacement profile.

$$u(x) = -\frac{P_t}{btE_C\omega\sinh(\omega L)}\cosh(\omega x) \quad \text{(8)}$$

The relationship between the load P_t and the measured displacement at the bottom surface of the concrete topping when x is equal to L can be expressed by Eq. 9.

$$P_t = -btE_C\omega\tanh(\omega L)u(L) \quad \text{(9)}$$

where $u(L)$ is the average in-plane displacement measured using LVDTs L3 and L4.

The measured P_t - $u(x)$ is simplified to a bilinear curve as shown in Fig 10. The slope k_{sm} was obtained such that areas A1 and A2 are equal. The coordinates of points C for all specimens are reported in Table 2 and were used to define P_t and $u(L)$ and then evaluate ω using Eq. 9.

Maximum Shear Stress ($v_{h\,max}$)

The in-plane displacement distribution along the X axis of the concrete topping can be obtained using Eq. 8. The horizontal shear stress distribution, v_h, can be then evaluated using Eq. 1. Fig. 11 illustrates the horizontal shear stress distribution along the X axis. Fig. 12 compares the calculated horizontal shear stress profile for slab B1 and the average measured horizontal shear stress at failure. The actual horizontal shear profile shows a concentration of the shear stresses near the applied load P_t. This observation indicates that the tested slabs sustained higher stresses than the average value. Table 1 shows the average and the calculated horizontal shear stress values at yielding. For all of the tested slabs, the shear strength at the interface between the hollowcore slabs and the concrete topping reached values that are much higher than the values specified in North American design standards.

Out-of-Plane Equilibrium

Fig. 9 illustrates the forces and stresses acting on element T in the out-of-plane direction. The external applied moment, *m(x)*, results from the eccentric force in the shear spring, F_s, and can be found by multiplying the force F_s by half the thickness of the concrete topping. The applied moment, *m(x)*, can be defined using Eq. 10.

$$m(x) = k_s \frac{bt}{2} u(x) \quad \text{(10)}$$

The force, F_p, is developed in the out-of-plane springs as a result of the applied moment *m(x)* and is responsible for the peel behavior of the concrete topping. F_p can be calculated from the equilibrium of forces along the Z axis and the equilibrium of the external and the internal moments acting on the element, Eqs. 11 and 12.

$$\frac{dV}{dx} = -k_p b w(x) \quad \text{(11)}$$

$$\frac{dM}{dx} = V + m(x) \quad \text{(12)}$$

Utilizing the moment-curvature relationship, Eq. 13, the differential equation governing the peel behavior, Eq. 14, can be derived.

$$M(x) = EI \frac{d^2 w}{dx^2}(x) \quad \text{(13)}$$

$$\frac{d^4 w(x)}{dx^4} + \lambda^4 w(x) = \frac{1}{EI} \frac{dm}{dx}$$

$$\ldots\ldots\ldots\ldots\ldots\ldots\ldots\ldots\ldots\ldots \text{(14a)}$$

where $\lambda^4 = \frac{bk_p}{EI}$ ………………..………………………..…………………………….. (14b)

The homogenous and particular solutions of Eq. 14 are given by Eq. 15.

$$w(x) = A\cos(\lambda x)\cosh(\lambda x) + B\cos(\lambda x)\sinh(\lambda x) + C\sin(\lambda x)\cosh(\lambda x) + D\sin(\lambda x)\sinh(\lambda x)\cos(\lambda x) - F\sinh(\omega x) \quad \text{(15a)}$$

where $F = \frac{\mathrm{P_t} k_s}{E_c^{\,2} I \, sinh(\omega L)(\lambda^4 + \omega^4)}$ ………..………………………………………….……...

(15b)

The constants *B* and *D* can be determined by applying the following boundary conditions at the free end of the concrete topping ($x = 0$).

(1) $\frac{d^2 w}{dx^2} = 0$ (M = 0).

(2) $\frac{d^3 w}{dx^3} = 0$ (V = 0).

Substituting with the evaluated constants, Eq. 15 reduces to the following form:

$$w(x) = A\cos(\lambda x)\cosh(\lambda x) + C[\cos(\lambda x)\sinh(\lambda x) + \sin(\lambda x)\cosh(\lambda x)] + \frac{F}{2}\frac{\omega}{\lambda}\cos(\lambda x)\sinh(\lambda x) + F\sinh(\omega x) \quad \text{(16)}$$

Eq. 16 represents the calculated out-of-plane displacement profile of the concrete topping, *w(x)*, and contains three unknowns *A*, *C* and λ. The load and displacement defining point C in Fig. 10 and the corresponding strains (point D in Fig. 13) are used to evaluate these constants as follows:

1- The values of $(du/dx)_{mid}$, Fig. 14, are evaluated at the locations of S1, S3 and S5 by differentiating Eq. 8.

2- Readings of S1, S3, and S5 represent the measured strain at the surface of the concrete topping, $(du/dx)_{outer}$, Fig. 14.

3- $(du/dx)_{bending}$ is evaluated at the locations of S1, S3, and S5 using Eq. 17.

$$\left(\frac{du}{dx}\right)_{bending} = \left(\frac{du}{dx}\right)_{outer} - \left(\frac{du}{dx}\right)_{mid} \quad \text{(17)}$$

4- The curvature of the concrete topping at the locations of S1, S3 and S5 is evaluated using Eq. 18.

$$\left(\frac{d^2w}{dx^2}\right) = -\frac{2}{t}\left(\frac{du}{dx}\right)_{bending} \quad \text{(18)}$$

5- The cubic function that best fits the calculated curvature in step 4 is then evaluated. Fig. 15 shows a typical cubic function.

6- The out-of-plane measured displacement profile $w(x)_m$ was obtained by double integration of Eq. 18. The two integration constants were then evaluated using the out-of-plane displacement readings from LVDTs L1 and L2.

7- Nonlinear regression analysis was conducted to match the calculated out-of-plane displacement profile $w(x)$ with the displacement profile $w(x)_m$ evaluated in step 6. This analysis allowed determining constants A, C and λ.

Shear and Peel Stiffnesses

The peel stiffness k_p is calculated using Eq. 14b by substituting with the value of λ. The out-of-plane profile, $w(x)$, is shown in Fig. 16 for all tested slabs. The shear stiffness k_s is calculated using Eq. 7. Table 3 presents the calculated shear and peel stiffnesses for all slab specimens. k_p is considerably smaller than k_s for all slabs. Average shear stiffnesses (k_s) of 50.8 (N/mm)/mm^2 and 6.8 (N/mm)/mm^2 and peel stiffnesses (k_p) of 7.2 (N/mm)/mm^2 and 2.0 (N/mm)/mm^2 were calculated for slabs from manufacturer A and B, respectively. Manufacturers A and B can use these values to predict the composite behavior of their hollowcore slabs.

SUMMARY AND CONCLUSIONS

Push-off tests that examine the shear and peel behavior at the interface between four hollowcore slabs and their concrete topping were presented in this paper. All of the slabs had a lightly-roughened surface finish using a conventional steel broom and achieved slightly higher average shear stresses than required by the North American design standards. Comparing the average shear results indicated that the shear strength considerably varies between hollowcore slabs from different manufacturers. An analytical model that simulates the interface between the hollowcore slab and the concrete topping using continuous springs was utilized. The springs depicted the interfacial shear and peel behaviors. The actual shear stresses were evaluated using the analytical model and found to be higher than the average measured values for all of the tested slabs. The actual values are much higher than the specified code limits. The shear and peel stiffnesses, k_s and k_p, of the interface between hollowcore slabs and concrete topping were then estimated using the presented analytical model. The reported k_s and k_p values are unique for the tested slabs. The presented method can be repeated to evaluate these stiffnesses for slabs from different manufacturers. Structural engineers can then use k_s and k_p values to evaluate the actual shear stresses developed at the interface between hollowcore slabs and their concrete topping and judge on the appropriateness of using the composite action.

5. ACKNOWLEDGMENTS

The authors would like to acknowledge the enthusiastic guidance and advice provided by Mr. Anil Mehta from The Prestressed Group (Windsor, ON). Appreciation is extended to the Canadian Precast/Prestressed Institute (CPCI) and the Ontario Centers of Excellence (OCE) for their financial and technical support.

REFERENCES

1. CSA A23.3-04 (2004). "Design of concrete structures." *Canadian Standard Association*, Mississauga, Canada.
2. ACI 318-08 (2008). "Building Code Requirements for Structural Concrete (ACI 318-08) and Commentary." *American Concrete Institute*, Michigan, United States.
3. Technical Bulletin 74-B6 (1974). "Composite Systems Without roughness." *Concrete Technology Association (CTA)*, CTA 35, pp 271-316.
4. Technical Bulletin 76-B4 (1976). "Composite Systems without Ties." *Concrete Technology Association (CTA),* CTA 36, pp 317-360.
5. Girhammar U.A. and Pajari M. (2008). "Tests and analysis on shear strength of composite slabs of hollow core units and concrete topping." *Construction and Building Materials*, 22, 1708-1722.
6. Ibrahim I. S. and Elliot K. S. (2006). "Interface Shear Stress of Hollow Core Slabs with Concrete Toppings." *Sixth International Conference on Concrete Engineering and Technology, (CONCET 2006)*, Institution of Engineers Malaysia, Kuala Lumpur, 104-116
7. El Damatty A.A. and Abushagur M. (2003). "Testing and modeling of shear and peel behavior for bonded steel/FRP connections." *Thin-Walled Structures*, 41, 987-1003.

8. CSA A23.1-09 (2009). “Concrete materials and methods of concrete construction.” *Canadian Standard Association*, Mississauga, Canada.
9. ASTM C349, (2008), “Standard Test Method for Compressive Strength of Hydraulic-Cement Mortars”, *ASTM International*, Pennsylvania, United States.
10. ASTM C39/C39M, (2005), “Standard Test Method for Compressive Strength of Cylindrical Concrete Specimens”, *ASTM International*, Pennsylvania, United States.

NOTATIONS

b: width of the concrete topping in the push-off tests, 508 mm

E_c: modulus of elasticity of concrete

f'_c: concrete compressive strength

F_s: in-plane force on element T in the X direction

F_p: out-of-plane force on element T

k_p: peel stiffness at the interface between the hollowcore slab and the concrete topping

k_s: shear stiffness at the interface between the hollowcore slab and the concrete topping

k_{sm}: slope of the measured load-displacement graph

L: length of the concrete topping in the push-off tests, 508 mm

M: internal moment in the concrete topping

$m(x)$: external applied moment on the concrete topping

P_{hc}: load applied on the hollowcore slab using the hydraulic actuator during the push-off test

P_p: load at the end of the linear stage, determined from the load-strain graphs

P_t: reaction on the concrete topping during the push-off tests

t: concrete topping thickness in the push-off tests, 50 mm

$u(x)$: in-plane displacement profile along the axis X

V: internal shear force in the concrete topping

$w(x)$: calculated out-of-plane displacement profile of the concrete topping

$w(x)_m$: measured out-of-plane displacement profile of the concrete topping

v_h: shear stress

$v_{h\ avg.}$: average measured shear stress

$v_{h\ max}$: maximum shear stress calculated using the analytical model

Table 1: Push-off test results

Specimen Label	Failure load, kN	Measured average shear strength, $v_{h\ avg.}$, MPa	Calculated yielding horizontal shear stress, $v_{h\ max.}$, MPa
A1	504	1.95	6.19
A2	554	2.15	7.24
B1	223	0.86	1.24
B2	182	0.71	1.01

Table 2: Values of P_t and $u(L)$ at the yielding points, C

Slab label	$\boldsymbol{P_t}$**, kN**	$\boldsymbol{u(L)}$**, mm**
A1	504	0.130
A2	554	0.134
B1	223	0.184
B2	182	0.148

Table 3: Shear and Peel stiffnesses

Specimen Label	Horizontal shear stiffness k_s, (N/mm)/mm^2	Peel stiffness k_p, (N/mm)/mm^2
A1	47.60	3.82
A2	54.00	2.96
B1	6.72	0.80
B2	6.85	1.06

LIST OF TABLES

Fig. 1: Lightly roughened hollowcore slabs,

a. Roughening method, b. Manufacturer A pattern, c. Manufacturer B pattern

Fig. 2: 50 mm cubes for compressive strength test

Fig. 3: Concrete topping

a. Formwork of concrete topping

b. Casting of concrete topping

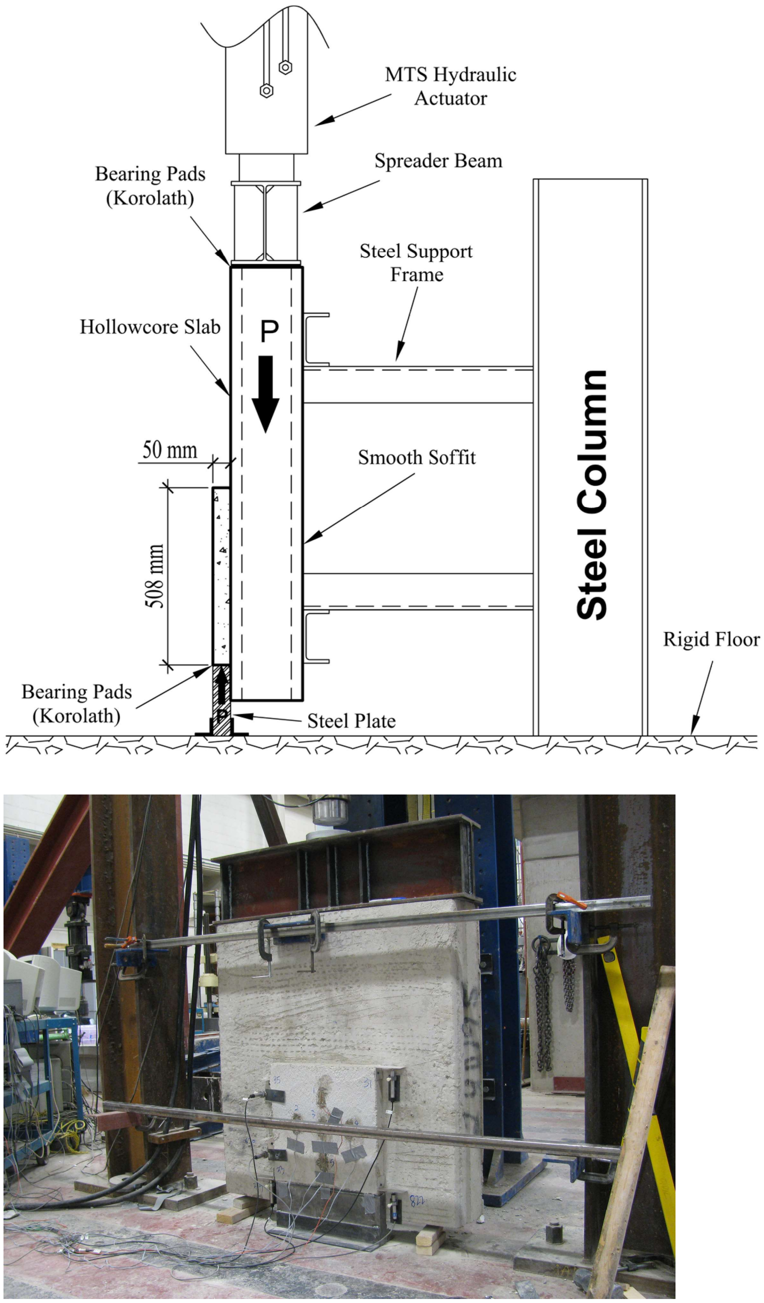

Fig. 4: Push-off test setup

a. Schematic

b. Photo

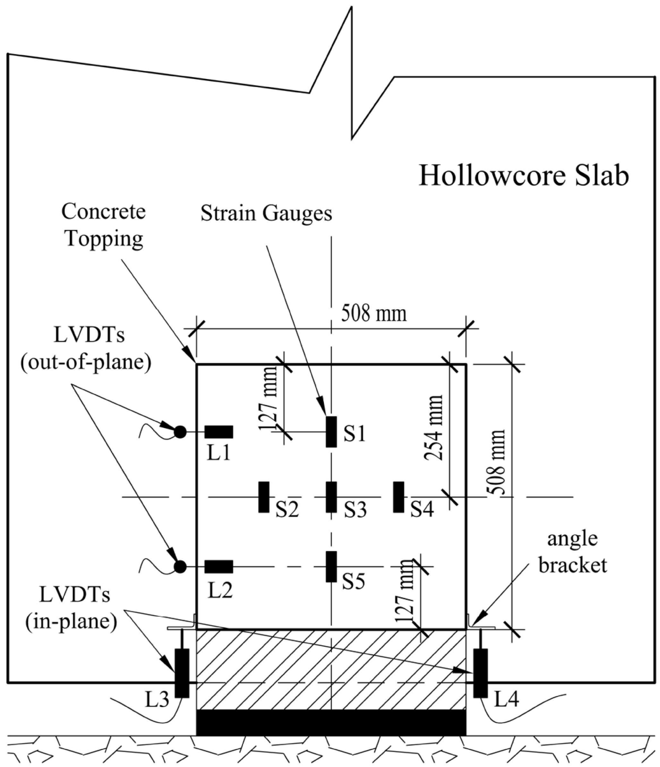

Fig. 5: Instrumentation

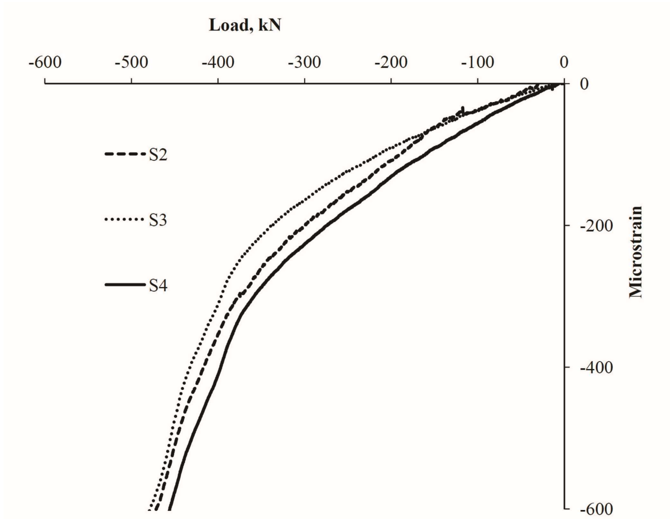

Fig. 6: Strain gauge readings for slab A1

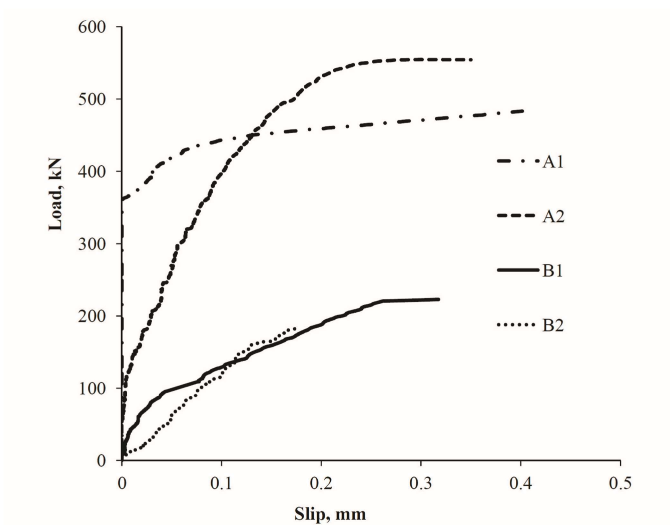

Fig. 7: Load-slip curves

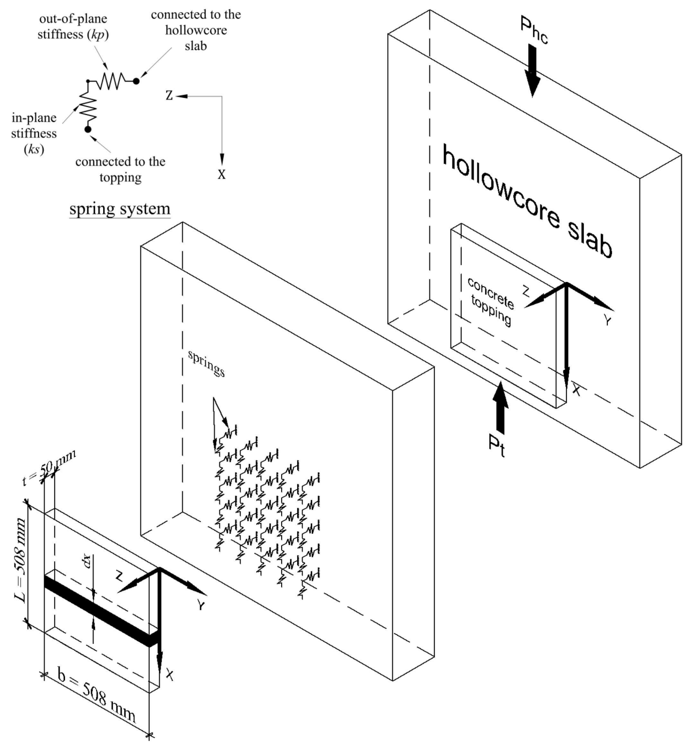

Fig. 8: General layout of the push-off test spring model

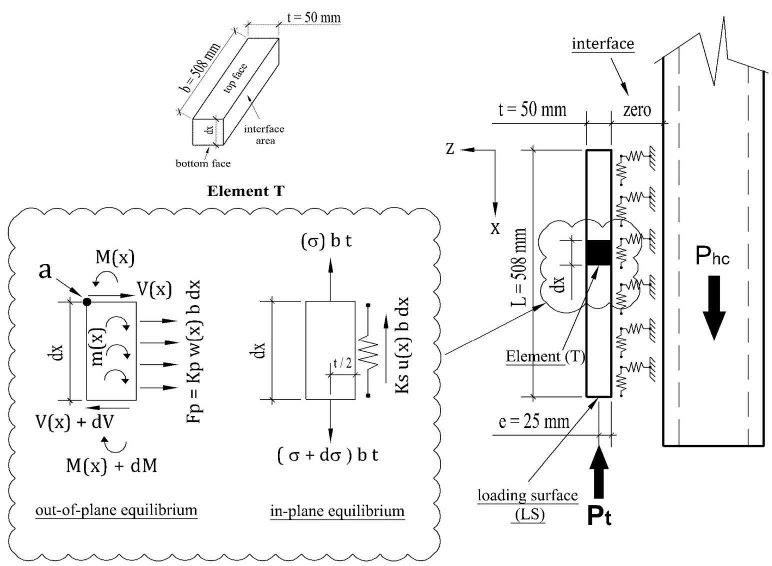

Fig. 9: Free body diagram of element T showing in-plane equilibrium

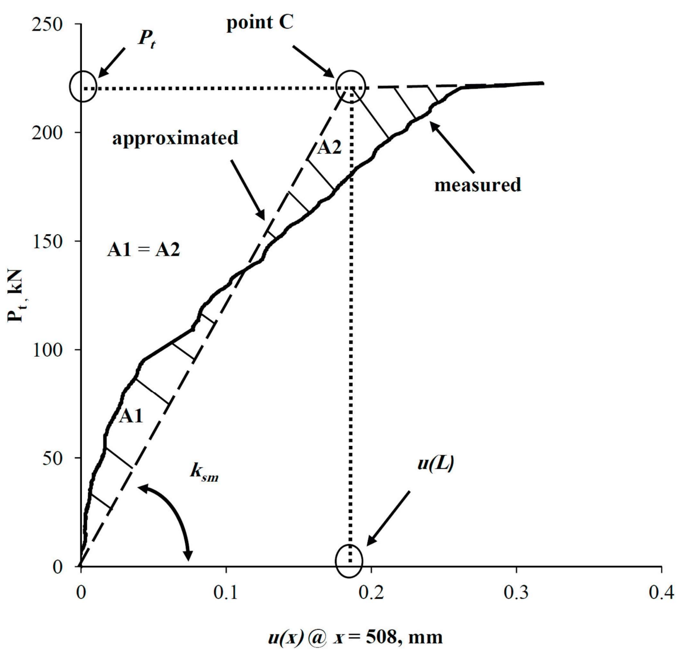

Fig. 10: Approximate load-slip relationship for slab B1 (typical)

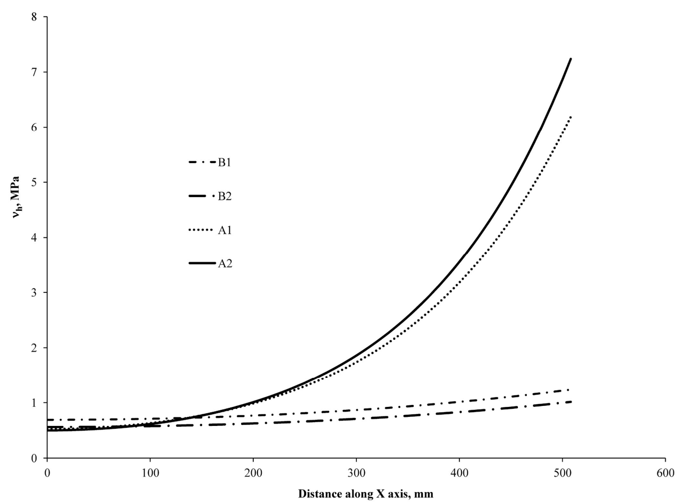

Fig. 11: Horizontal shear stress distribution

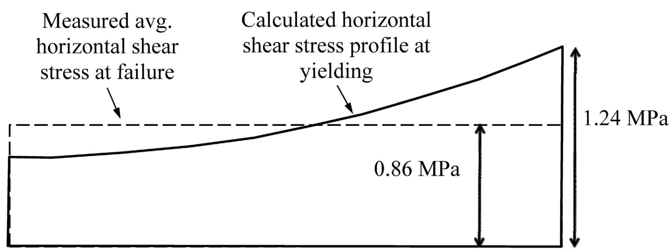

Fig. 12: Horizontal shear stress distribution for slab B1 (typical)

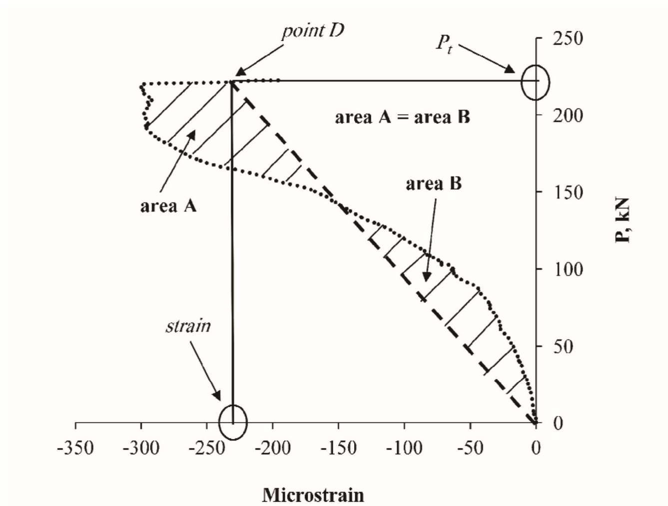

Fig. 13: Approximate load-S3 strain relationship for slab B1 (typical)

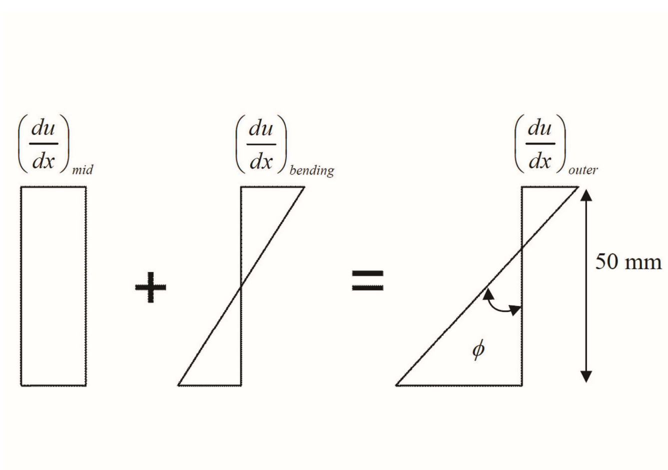

Fig. 14: State of strains in the concrete topping

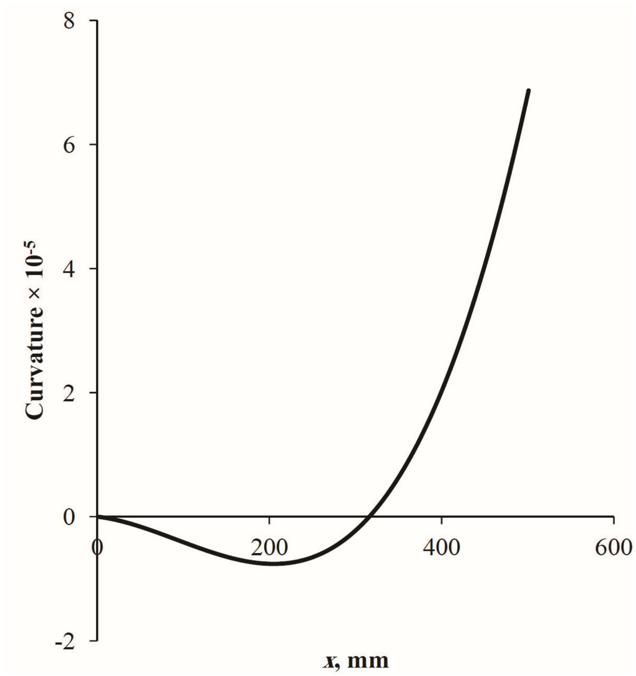

Fig. 15: Curvature best fit cubic curve

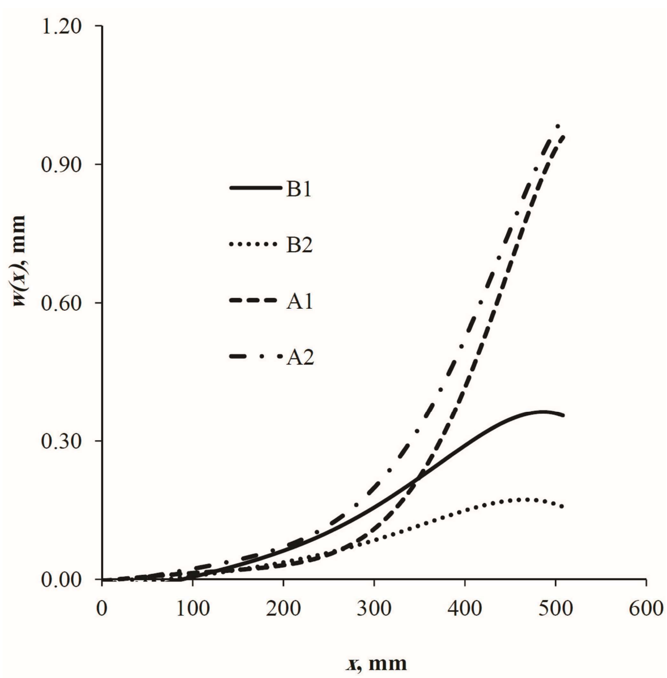

Fig. 16: Out-of-plane displacement profiles